# Effects of Fluid–Fluid Interfacial Elasticity on Droplet Formation in Microfluidic Devices

**Chun-Xia Zhao**
Centre for Biomolecular Engineering, Australian Institute for Bioengineering and Nanotechnology, The University of Queensland, St. Lucia, QLD 4072, Australia

**Erik Miller**
Tissue Engineering and Microfluidics Laboratory, Australian Institute for Bioengineering and Nanotechnology, The University of Queensland, St. Lucia, QLD 4072, Australia

**Justin J. Cooper-White**
Tissue Engineering and Microfluidics Laboratory, Australian Institute for Bioengineering and Nanotechnology, The University of Queensland, St. Lucia, QLD 4072, Australia, and

School of Chemical Engineering, The University of Queensland, St. Lucia, QLD 4072, Australia

**Anton P. J. Middelberg**
Centre for Biomolecular Engineering, Australian Institute for Bioengineering and Nanotechnology, The University of Queensland, St. Lucia, QLD 4072, Australia, and

School of Chemical Engineering, The University of Queensland, St. Lucia, QLD 4072, Australia

*DOI 10.1002/aic.12382*
*Published online August 16, 2010 in Wiley Online Library (wileyonlinelibrary.com).*

*Biomolecules adsorb at fluid–fluid interfaces and can form a cohesive interfacial network imparting distinctive local interfacial mechanics. This modification of interfacial behavior is empirically known to significantly affect the stability and flow behavior of foams and emulsions. Droplet formation in the presence of interfacial networks is investigated in a flow-focusing microfluidic device using designed peptide surfactants, which allow decoupled control of interfacial rheology and interfacial tension. The influence of interfacial elasticity on droplet breakup, satellite droplet formation and droplet size are reported. The presence of high interfacial elasticity strongly affects the mechanism of droplet breakup by delaying neck thinning and altering interfacial shape at the point of droplet detachment, resulting in the suppression of satellite droplet formation and a decrease in droplet size. We report a correlation between dimensionless droplet size and a new dimensionless grouping which combines flow-rate ratio with the ratio of interfacial tension and interfacial elasticity.*
 *AIChE J,* 57: 1669–1677, 2011
*Keywords: microfluidics, droplet formation, interfacial rheology, peptide, interfacial elasticity*

## Introduction

Emulsions, dispersions of one dispersed liquid in another continuous liquid, are widely used in products including foods, cosmetics, and pharmaceuticals. The droplet size and size distribution of emulsions are generally regarded as important properties affecting the stability, rheology, and chemical reactivity of any emulsion. Although numerous emulsification techniques are available, including high-pressure homogenizers, ultrasound homogenizers and rotor/stator systems such as stirred vessels, colloid mills and toothed disc

Correspondence concerning this article should be addressed to A. P. J. Middelberg at a.middelberg@uq.edu.au

dispersing machines,[1] most result in emulsions having a wide size distribution. Demand for near monodisperse emulsion technologies has increased in recent years due to new advances in the production of microcapsules and the search for multiphase systems where unique function is imparted by multiscale structural control. Microfluidic droplet production is now a well-established technology for producing desirable near monodisperse emulsions.[2,3] Monodisperse droplets in microfluidic devices have been generated via a number of geometries including T-junctions,[4–7] co-flowing including flow-focusing[2,8–13] and straight-through microchannel designs (MC).[14,15]

A number of studies have been conducted to investigate the mechanisms of droplet formation in microfluidic devices.[7,16,17] The geometric features of the device have been shown to strongly affect the mechanism of droplet formation. The type and physical properties of the dispersed and continuous phase, including viscosity and interfacial tension, also greatly influence droplet formation behavior and final droplet size.[18] The T-junction geometry exploits a shear-rupturing mechanism in which the size of the droplets is controlled by the interplay of shear stress and interfacial tension[6] represented by the capillary number, $Ca$ ($=v\mu/\sigma$, where $v$ and $\mu$ are the continuous-phase velocity and dynamic viscosity, respectively, and $\sigma$ is interfacial tension). In flow-focusing geometries, the process of break-up and droplet size are determined largely by the ratio of the volumetric flow rates of the dispersed phase ($Q_d$) to the continuous phase ($Q_c$).[17] In both methods, droplet break-up is influenced by instabilities at the fluid–fluid interface, which are in turn affected by high concentrations of surface active agents which can control interfacial rheology. In particular, biological macromolecules including proteins and peptides both reduce interfacial tension and impart a distinct cohesive character to the interface.[19–22] From bulk emulsification studies it is known that such rheologically complex interfaces affect droplet breakup in a way that is not well represented simply by the capillary number.[23] Despite the wide application of biologically complex fluids in microfluidic devices, no studies have reported the effects of interfacial rheology on droplet formation in such systems. In part this limitation arises because it is difficult to experimentally alter interfacial rheology without simultaneously changing interfacial tension and macromolecular composition.

Peptides have been developed in recent years as building blocks for novel materials encoding stimuli-responsive behavior; certain designs based on a heptad $\alpha$-helix motif have been shown to act as surfactants.[24] These peptide surfactants can be designed to self-assemble at a fluid–fluid interface to create a molecularly thin network that, in the presence of metal ions, has a Young's modulus similar to collagen.[25] Switching between this mechanically strong cohesive film and a mobile detergent-like nonfilm state can be rapidly achieved by the addition of chelating agent or acid to the bulk solution, without significantly changing interfacial tension.[26,27] The interfacial rheology of peptide surfactants AM1[26] and AFD4[28] in the cohesive film state is similar to that for protein-coated interfaces, while in the absence of metal ions these peptide surfactants impart very low interfacial elasticity and behave qualitatively similar to small chemical surfactants [such as sodium dodecyl sulfate, (SDS)]. The surface excess and hence interfacial tension of these peptide surfactants changes very little as the interface is triggered to change between the high and low elasticity states,[25] providing an unprecedented ability to vary interfacial rheology without significantly changing interfacial tension and macromolecular composition.

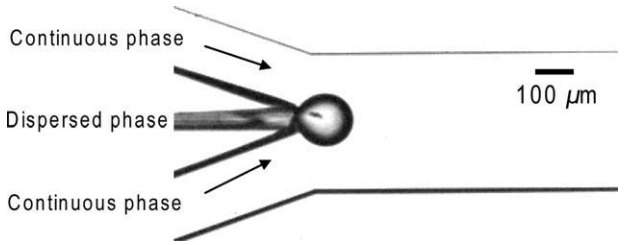


**Figure 1. Micrograph of the flow-focusing microfluidic device.**

In this study, we detail a systematic microfluidic study of droplet formation in the presence of these two peptide surfactants. To distinguish the effects of interfacial elasticity from those due to interfacial tension, results are compared with those for droplet formation in the presence of a small molecular weight surfactant, SDS, which in contrast to the peptide surfactants imparts negligible interfacial elasticity. This study reports the influence of interfacial elasticity on the dynamics of neck thinning and the formation of satellite droplets, and correlates final droplet size with a new dimensionless grouping that incorporates interfacial tension and interfacial elasticity as correlating variables.

## Experimental

### *Microfluidic device*

Experiments were performed in a flow-focusing microfluidic device, which was fabricated from poly(dimethylsiloxane) (PDMS) using standard soft-lithography and SU-8 photolithography techniques, and bonded to PDMS-coated glass coverslips to provide uniform surface properties on all walls of the channel. Details of the specific fabrication procedure were reported elsewhere.[29] Figure 1 shows a picture of the flow-focusing microfluidic device. The continuous (oil) phase flows through the two side channels (width 160 $\mu$m) and the dispersed (aqueous) phase is introduced via the central channel (width 40 $\mu$m). The three streams meet at the focusing point. The downstream channel has width 400 $\mu$m; the depth of the device is 150 $\mu$m.

### *Materials*

Peptides AM1 (MW 2473, Ac-MIKQLADS LHQLARQ VSRLEHA-$CONH_2$)[26] and AFD4 (MW 2435, Ac-MKQLADS LHQLAHK VSHLEHA-$CONH_2$)[28] were synthesized by GenScript Corporation (Piscataway, NJ). The purity of each peptide was >95% by reversed-phase high-performance liquid chromatography (RP-HPLC). The peptide content of lyophilized samples was determined by quantitative amino acid analysis (Australian Proteome Analysis Facility, Sydney). The 12 systems detailed in Table 1 were chosen to systematically investigate the dynamics of droplet formation in the microfluidic device. Miglyol 812 oil (viscosity $\mu = 30$ mPa s, and density $\rho = 950$ kg/m$^3$, Sasol GmbH, Germany) was purified using a silica column and was used as the

**Table 1. Continuous and Dispersed Phases Used in this Study and Their Reference Names**

| Continuous Phase | Dispersed Phase | Surfactant in the Dispersed Phase | System Name |
|---|---|---|---|
| Miglyol 812 oil | MilliQ water | 3.88 mM SDS | 3.88 mM SDS |
| | | 6.59 mM SDS | 6.59 mM SDS |
| | | 100 $\mu$M AFD4, 200 $\mu$M EDTA, pH 7.0 | AFD4+EDTA |
| | | 100 $\mu$M AFD4, 200 $\mu$M $ZnCl_2$, pH 7.0 | AFD4+$ZnCl_2$ |
| | | 100 $\mu$M AFD4, 200 $\mu$M $ZnSO_4$, pH 7.0 | AFD4+$ZnSO_4$ |
| | | 100 $\mu$M AM1, 200 $\mu$M EDTA, pH 7.0 | AM1+EDTA |
| | | 100 $\mu$M AM1, 200 $\mu$M $ZnCl_2$, pH 7.0 | AM1+$ZnCl_2$ |
| | | 100 $\mu$M AM1, 200 $\mu$M $ZnSO_4$, pH 7.0 | AM1+$ZnSO_4$ |
| | 30 wt.% glycerol-water mixture | 100 $\mu$M AFD4, 200 $\mu$M EDTA, pH 7.0 | 30% Glyc AFD4+EDTA |
| | | 100 $\mu$M AFD4, 200 $\mu$M $ZnSO_4$, pH 7.0 | 30% Glyc AFD4+ $ZnSO_4$ |
| | 50 wt.% glycerol-water mixture | 100 $\mu$M AFD4, 200 $\mu$M EDTA, pH 7.0 | 50% Glyc AFD4+EDTA |
| | | 100 $\mu$M AFD4, 200 $\mu$M $ZnSO_4$, pH 7.0 | 50% Glyc AFD4+$ZnSO_4$ |

continuous phase since it does not swell the PDMS microchannels. The six aqueous peptide AM1 and AFD4 solutions (100 $\mu$M, pH 7.0, in the presence of 200 $\mu$M EDTA, $ZnCl_2$ or $ZnSO_4$), two SDS solutions (3.88 mM SDS and 6.59 mM SDS), and four glycerol/peptide systems were used as the dispersed phase to comparatively study the influence of interfacial elasticity on droplet formation. All peptide AM1 and AFD4 solutions were used within 12 h of preparation. All reagents and chemicals were of analytical grade. Water was from a MilliQ system (Millipore, North Ryde, Australia) equipped with a 0.22 $\mu$m filter had resistivity >18.2 M$\Omega$ cm. All glassware used in the experiment was cleaned by first soaking in a detergent solution (1% v/v Decon-90, Decon laboratories, Hove, UK), followed by rinsing with water, soaking for 10 min in freshly prepared piranha solution [equal parts of 30% (v/v) $H_2O_2$ and 98% (v/v) sulfuric acid], followed by copious rinsing with water.[28]

### *Visualization and analysis*

A Nikon inverted microscope (TE2000, Nikon) coupled with a phase contrast condenser was used for observation. Images were captured and processed using a high-speed camera (Phantom V, Vision Research) which can capture up to 5300 fps at 256 $\times$ 256 pixel resolution. SGE glass syringes, 1 mL and 500 $\mu$L, were used for the continuous and the dispersed phase flows, respectively. Flow rates of the continuous and dispersed phases were controlled using motor-driven syringe pumps (PHD2000 Harvard, Instech). After changing any of the flow parameters, we allowed at least 100 s of equilibration time before recording images for analysis. The droplet size ($d$) is determined by measuring the size of droplets from recorded pictures using Phantom camera control software (Vision Research, Wayne New Jersey).

### *Interfacial tension measurement*

The interfacial tensions of water-oil interfaces (of all the 12 systems in Table 1) were measured with a Krüss Drop Shape Analysis System DSA10 (Krüss GmbH, Hamburg, Germany). Miglyol 812 oil was filled into an 8 mL quartz cuvette, and water droplets (about 50 $\mu$L) were formed in the oil from a needle of known diameter (1.507 mm). The interfacial tension is measured by analyzing the static pendant drop shape, and readings were made every 5 s over 1000 s following initial droplet formation. The accuracy for interfacial tension measurement by this method is $\pm$0.01 mN/m. The equilibrium interfacial tension values were determined through the extrapolation via $\sigma(1/\sqrt{t})$ plot to infinite time based on the so-called long-time approximation for diffusion-controlled adsorption.[30,31]

### *Interfacial rheology measurements*

The dynamic interfacial rheology was measured with a profile analysis tensiometer (PAT1) from Sinterface (Berlin, Germany) for the 12 systems in Table 1. A pendant water droplet was formed at the tip of a stainless steel capillary in Miglyol 812 oil. Once equilibrium levels of adsorption were approached (that is, the interfacial tension stopped decreasing), measurement of dilatational elasticity and viscosity was performed. Droplet oscillation was achieved with the tensiometer automatic dosing system. The dynamic shape changes of an oscillating droplet were recorded, and were then analyzed with a Fourier transform function to extract the interfacial rheology. Oscillations of droplets were performed with sinusoidal perturbations at a frequency of 0.2 Hz and at 1% amplitude. The instrument accuracy is $\pm$0.1 mN/m.

## Results and Discussion

The range of fluids investigated (Table 1) allowed for a systematic experimental study of the effects of interfacial elasticity and viscosity on droplet formation and break-up dynamics in a flow-focusing microfluidic device. The six peptide AM1 and AFD4 solutions spanned a wide range of interfacial elasticity; the two SDS systems were used as reference solutions having interfacial tension similar to the peptide surfactant solutions, but with minimal interfacial elasticity. The four glycerol/peptide solutions allowed the influence of viscosity, and its interaction with interfacial elasticity, to be probed.

### *Interfacial rheology characterization*

The equilibrium interfacial tensions of the 12 solutions defined in Table 1, obtained by drop shape analysis, are shown in Table 2. SDS solution at 3.88 mM was used as a reference solution for the AM1+$ZnSO_4$ system and the 6.59 mM SDS solution for the AFD4+$ZnSO_4$ system, as they have similar equilibrium interfacial tensions. The rheological properties of the surfactant- or peptide-coated oil-water

**Table 2. Interfacial Tension and Interfacial Rheology of Solutions Defined in Table 1**

| System Name | Interfacial Tension (mN/m) | Interfacial Elasticity (mN/m) | Interfacial Viscosity (mN·s/m) |
|---|---|---|---|
| 3.88 mM SDS | 11.6 ± 0.1 | 2.0 ± 0.4 | 0.7 ± 0.3 |
| 6.59 mM SDS | 6.33 ± 0.05 | 2.0 ± 0.2 | 1.2 ± 0.2 |
| AFD4+EDTA | 10.2 ± 0.1 | 4.7 ± 0.2 | 3.5 ± 0.6 |
| AFD4+$ZnCl_2$ | 6.9 ± 0.1 | 19 ± 3 | 14 ± 2 |
| AFD4+$ZnSO_4$ | 6.3 ± 0.1 | 39 ± 5 | 21 ± 1 |
| AM1+EDTA | 11.6 ± 0.1 | 2.8 ± 0.3 | 1.8 ± 0.2 |
| AM1+$ZnCl_2$ | 11.6 ± 0.2 | 4.5 ± 0.5 | 1.5 ± 0.5 |
| AM1+$ZnSO_4$ | 12.0 ± 0.2 | 6.0 ± 0.2 | 1.5 ± 0.7 |
| 30% (w/w) Glyc AFD4+EDTA | 14.7 ± 0.2 | 3.3 ± 0.3 | 1.8 ± 0.1 |
| 30% Glyc AFD4+$ZnSO_4$ | 12.6 ± 0.1 | 55 ± 2 | 11 ± 3 |
| 50% Glyc AFD4+EDTA | 13.23 ± 0.06 | 43 ± 6 | 16 ± 4 |
| 50% Glyc AFD4+$ZnSO_4$ | 10.55 ± 0.05 | 37 ± 3 | 1.0 ± 0.3 |

interface were determined using the PAT1. The PAT1 is widely used to investigate interfacial viscoelastic properties by harmonically changing the volume of bubbles or droplets, although the viscoelastic parameters at even 5% amplitude are unreliable for highly elastic interfaces.[32] In this study a minimal 1% amplitude was therefore used. Within the instrument accuracy of ±0.1 mN/m, there was no significant change in the interfacial tension of SDS solutions with droplet volume dilation, suggesting low values of interfacial elasticity and interfacial viscosity, as reported in Table 2. The interfacial tensions of the six peptide AM1 and AFD4 solutions and the four glycerol/peptide solutions versus time are shown in Figures 2a, b, respectively. Interfacial tension varies slightly with droplet volume for AM1 systems, AFD4+EDTA and the 30% glycerol AFD4+EDTA system. For AFD4+$ZnCl_2$, AFD4+$ZnSO_4$, 30% glycerol AFD4+$ZnSO_4$, 50% glycerol AFD4+EDTA, and 50% glycerol AFD4+$ZnSO_4$ systems (Figure 2), interfacial tension was strongly dependent on droplet volume, and the Fourier transform of the cyclic dynamic interfacial tension suggested a high dilatational elasticity, as shown in Table 2. The interfacial elasticity of the peptide layers varies significantly in the presence of either EDTA, $ZnCl_2$ or $ZnSO_4$. For the two very high viscosity systems (50% glycerol AFD4+EDTA and 50% glycerol AFD4+$ZnSO_4$) the measured interfacial elasticity values are similar, contrary to the known behavior for AFD4 in simple aqueous solutions whereby elasticity increases substantially in the presence of Zn(II). This result is simply due to the measurement principle of the PAT1. High interfacial tension gradients, as a result of slowed peptide adsorption due to high solution viscosity, manifest as high apparent values of interfacial elasticity. In contrast to the peptide solutions, SDS reference solutions impart negligible interfacial elasticity even with very similar equilibrium interfacial tension values.

The solutions investigated (Table 2) access a wide range of interfacial behaviors. Significant variation in interfacial elasticity for these solutions was qualitatively confirmed by observing a droplet undergoing rapid interfacial contraction (Figure 3). A droplet shape tensiometer (DSA-10, Krüss

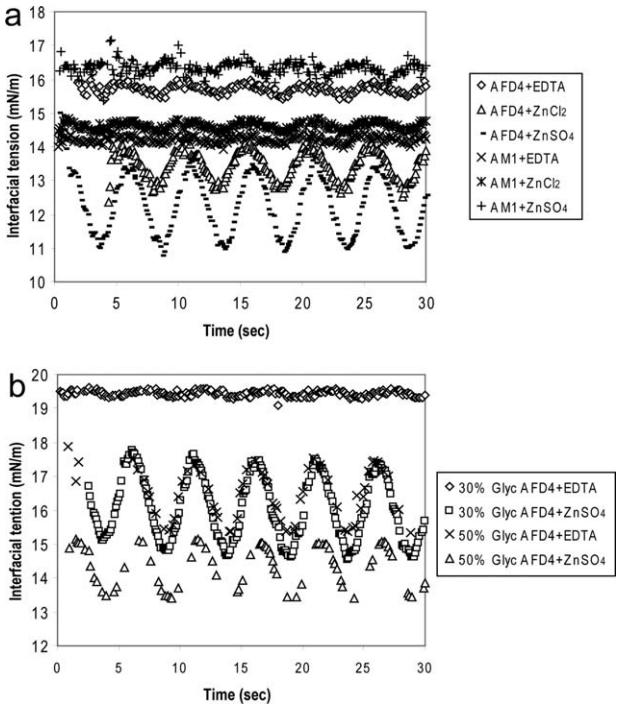


**Figure 2. Cyclic interfacial tension for peptide droplets versus time.**

(a) Peptide systems; (b) Glycerol/peptide systems.

GmbH, Hamburg, Germany) was used to record videos of peptide- and SDS-stabilized aqueous droplets formed from a straight needle fitted to syringe (SGE Analytical Science Pty, Ringwood Australia) and submerged in an 8 mL quartz cuvette (Hellma GmbH, Mülheim, Germany) filled with Miglyol 812 oil. Droplets (~10 μL) were aged for 10 min, and then a sudden reduction in the droplet volume was performed by withdrawing solution back into the syringe. In the presence of AFD4+$ZnSO_4$ or AM1+$ZnSO_4$, wrinkles formed on the water-in-oil droplet surface when the droplet volume was rapidly reduced, as seen in Figures 3b, e, reflecting a film of

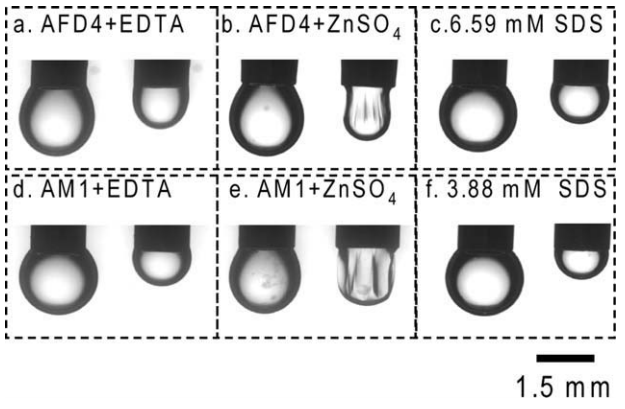


**Figure 3. Response of a pendant water droplet in Miglyol 812 oil during interfacial contraction in the presence of different surfactant formulations.**

Left: original droplet; Right: after deflation.

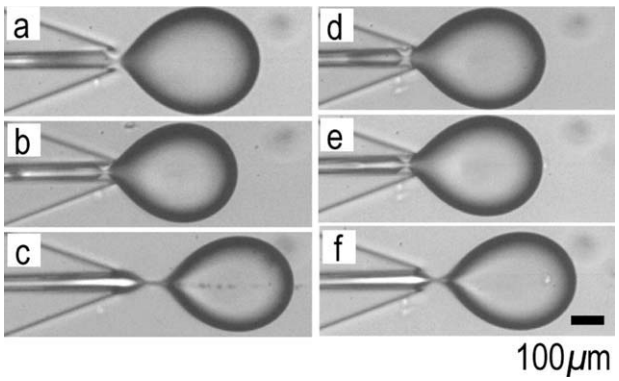


**Figure 4. Representative images of droplet formation in the flow-focusing device of Figure 1, for different aqueous-phase compositions at a flow rate ratio of $Q_d/Q_c = 0.05/2$ (mL/h)/(mL/h).**

(a) AFD4+EDTA; (b) AFD4+$ZnSO_4$; (c) 6.59 mM SDS; (d) AM1+EDTA; (e) AM1+$ZnSO_4$; (f) 3.88 mM SDS.

significant interfacial strength and rigidity (Table 2). In the case of AFD4+EDTA, AM1+EDTA, and SDS (Figures 3a, c, d, and f), instead of skin-like wrinkles, the interface remained smooth throughout the deflation process, even though AFD4+$ZnSO_4$ and 6.59 mM SDS have approximately the same interfacial tension, as do AM1+$ZnSO_4$ and 3.88 mM SDS.

### *Microfluidic droplet formation*

Droplet formation experiments were performed in a PDMS flow-focusing microfluidic device (Figure 1) with Miglyol 812 oil as the continuous phase, and aqueous solutions detailed in Table 1 as the dispersed phase. Both the flow rates of the continuous $Q_c$ (0.5, 1, 1.5, 2, 4 mL/h) and dispersed $Q_d$ (0.02, 0.1, 0.5 mL/h) phases were varied. The two side channels carry the continuous phase and the central channel supplies the dispersed phase. A typical process of droplet formation in this flow-focusing channel is as follows: the stream of the dispersed phase penetrates into the main channel, and the expansion decelerates the flow of the dispersed phase. The interfacial tension produces a nearly spherical bulb at the tip of the central channel. The bulb is fed by the dispersed phase source and grows gradually. Finally, a neck forms, and the droplet breaks up and is conveyed downstream. Then the dispersed stream retracts into the disperse phase channel and a new cycle commences. Two distinct stages exist during the droplet formation process: first, rapid expansion of the growing droplet; second, a fast elongation of the droplet until its rupture. For the first stage, the six systems in Figure 3 displayed the same behavior; the droplet expands spherically at the beginning of its formation and grows without significant movement in the continuous phase flow direction. Subsequently, in the second stage, the effect of flow inertia and shear stress become increasingly important during the growth of the droplet, and as the interface moves, the droplet is stretched to form a neck that is elongated to a teardrop shape until rupture. It is during this stage that the interfacial elasticity starts to influence droplet formation dynamics. The presence of a cohesive interfacial network prevents the droplet from moving along the fluid stream, and delays the movement of the interface. As a result, the breakup position of the AFD4+$ZnSO_4$ and AM1+$ZnSO_4$ solutions is different to that of AFD4+EDTA, AM1+EDTA, and SDS systems. The typical qualitative features of droplet formation immediately following droplet detachment are shown in Figure 4. The two SDS systems [Figures 4c, f] display notably different behavior to AFD4+$ZnSO_4$ (Figure 4b) and AM1+$ZnSO_4$ (Figure 4e), despite similar interfacial tensions (Table 2). For SDS, breakup occurs outside of the capillary and occurs with a longer filament, in contrast to peptide-surfactant controlled breakup [Figures 4b and e], which occurs within the capillary.

To more fully explore the breakup process in a quantitative way, the dynamics of neck thinning were recorded using a high-speed camera (Figure 5). As thinning progresses, the low elasticity AFD4+EDTA and 6.59 mM SDS systems show similar droplet break-up behavior, developing a long filament having rounded ends. In contrast, the high elasticity AFD4+$ZnSO_4$ system shows that the droplet instead breaks up with "pointed" ends, and these persist even after several hundred microseconds, suggesting a significant impact of interfacial elasticity on droplet dynamics. When we measured the minimal neck width as a function of time (Figure 5b), it was found that during the initial stage, the three systems exhibit identical initial thinning dynamics. However, at about half of the total breakup time, the AFD4+EDTA and 6.59 mM SDS systems start to diverge from the highly elastic AFD4+$ZnSO_4$ system. For the solution which assembles

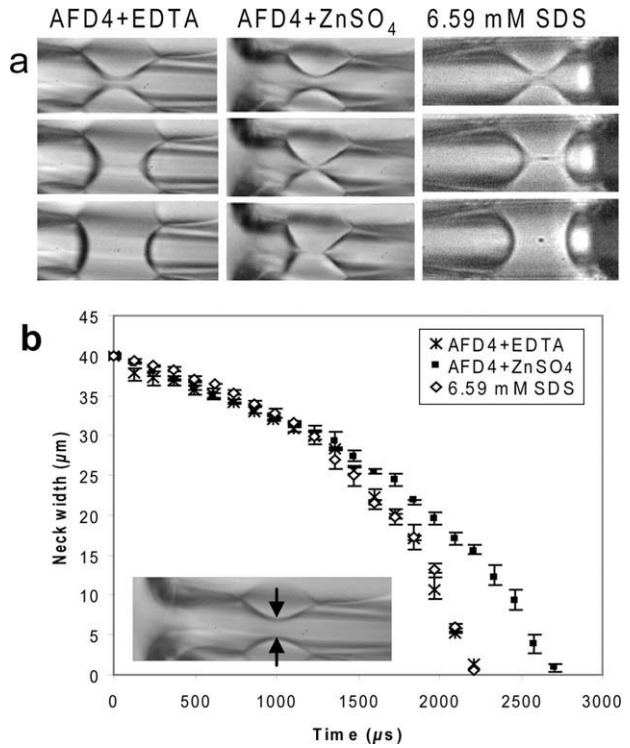


**Figure 5. Neck dynamics during droplet formation.**

(a) Minimal neck width in the capillary of the flow-focusing microchannel at a flow rate ratio of $Q_d/Q_c = 0.05/0.1$ (mL/h)/(mL/h); (b) Neck width as a function of time at $Q_d/Q_c = 0.05/0.1$ (mL/h)/(mL/h).

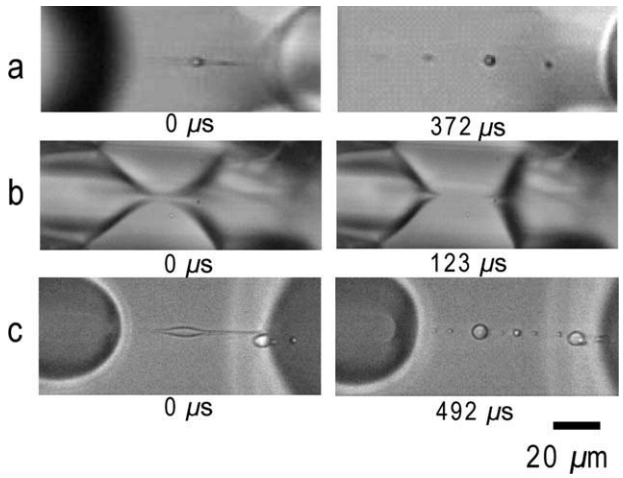


**Figure 6. Satellite droplet formation in a flow-focusing microfluidic device ($Q_d/Q_c$ = 0.5 (mL/h)/4 (mL/h)).**

(a) AFD4+EDTA; (b) AFD4+$ZnSO_4$; (c) 6.59 mM SDS.

a cohesive film having high interfacial elasticity (i.e., AFD4+$ZnSO_4$), break-up is slowed by about 500 $\mu$s. This trend is also found in other microfluidic-based droplet formation experiments using dilute polymer solutions (of polyethylene oxide), with the filament lasting at least an order of magnitude longer before breakup.[33,34]

### *Satellite formation*

Previous studies of microfluidic emulsification have observed that droplet pinch off leads to an array of uniformly large droplets, with smaller "satellites" in between.[16,35] The presence of satellite droplets is a significant problem in emulsification as it reduces droplet population homogeneity. The generation of satellite droplets is initiated by an imbalance in capillary forces during the break-off of the primary droplet. Surfactants, though vital for stable emulsion formation, dampen and suppress surface instabilities when present at low concentration. The accumulation of surfactants at the droplet surface therefore helps stabilize the rapidly stretching thread during droplet breakup, thus increasing the volume of liquid in the thread and ultimately resulting in the formation of satellite droplets.[36] Figure 6 shows satellite droplet formation for three systems (AFD4+EDTA, AFD4+$ZnSO_4$, and 6.59 mM SDS) in the flow-focusing microfluidic device. For AFD4+EDTA, which has a higher interfacial tension (Table 2) than 6.59 mM SDS, there are three small secondary droplets. For the system having highest interfacial elasticity AFD4+$ZnSO_4$, no (observable) satellite droplets were generated even though the interfacial tension is similar to that of 6.59 mM SDS (Table 2).

On examining the satellite droplet formation process it was noted that the 6.59 mM SDS and AFD4+$ZnSO_4$ solutions reveal two totally different mechanisms of breakup. For both systems, a neck is initially formed as seen in Figure 7. At this stage, the three systems mentioned above show a similar thinning process as confirmed by Figure 5b. However, at half of the breakup time, for AFD4+EDTA and 6.59 mM SDS, the motion of the liquids in the central neck reverses its direction which produces two pinch-offs from either side of the neck, which eventually contracts into a large slender filament aligned to the axis, as seen in Figure 7. The slender filament then pinches off at many locations due to interfacial tension force, thus giving birth to a string of small satellite drops.[37] For the system having highest interfacial elasticity (AFD4+$ZnSO_4$), the breakup process is totally different. The neck keeps decreasing in width and finally breakup occurs at the midpoint with pointed ends at each side. As a result, no satellite droplets are generated. From this study, it can be concluded that high interfacial elasticity suppresses satellite formation, suggesting that peptide surfactants may be used to increase the homogeneity of droplets formed during microfluidic emulsification.

### *Droplet size correlation*

With the qualitative aspects of the droplet formation mechanism characterized, the quantitative aspects of the variation in droplet size was considered, to investigate how the sizes of droplets formed in the device depend on the flow rates of each phase, interfacial tension, and interfacial elasticity. Only the primary droplet size was analyzed, as the largest satellite droplet size is about 2 $\mu$m, which is too small to be measured accurately compared to the primary droplet size of several hundred micrometers. A detailed experimental investigation of droplet size was carried out with the 12 systems listed in Table 2. Both the continuous (0.5,

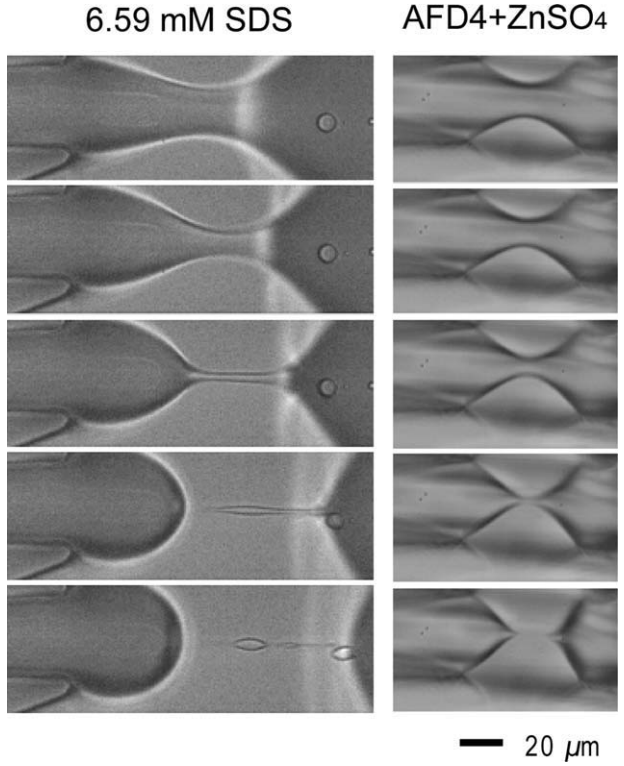


**Figure 7. Time evolution leading to the pinch-off of droplets ($Q_d/Q_c$ = 0.5 (mL/h)/4 (mL/h)).**

Time interval for 6.59 mM SDS images is 246 $\mu$s and for AFD4+$ZnSO_4$ is 123 $\mu$s.

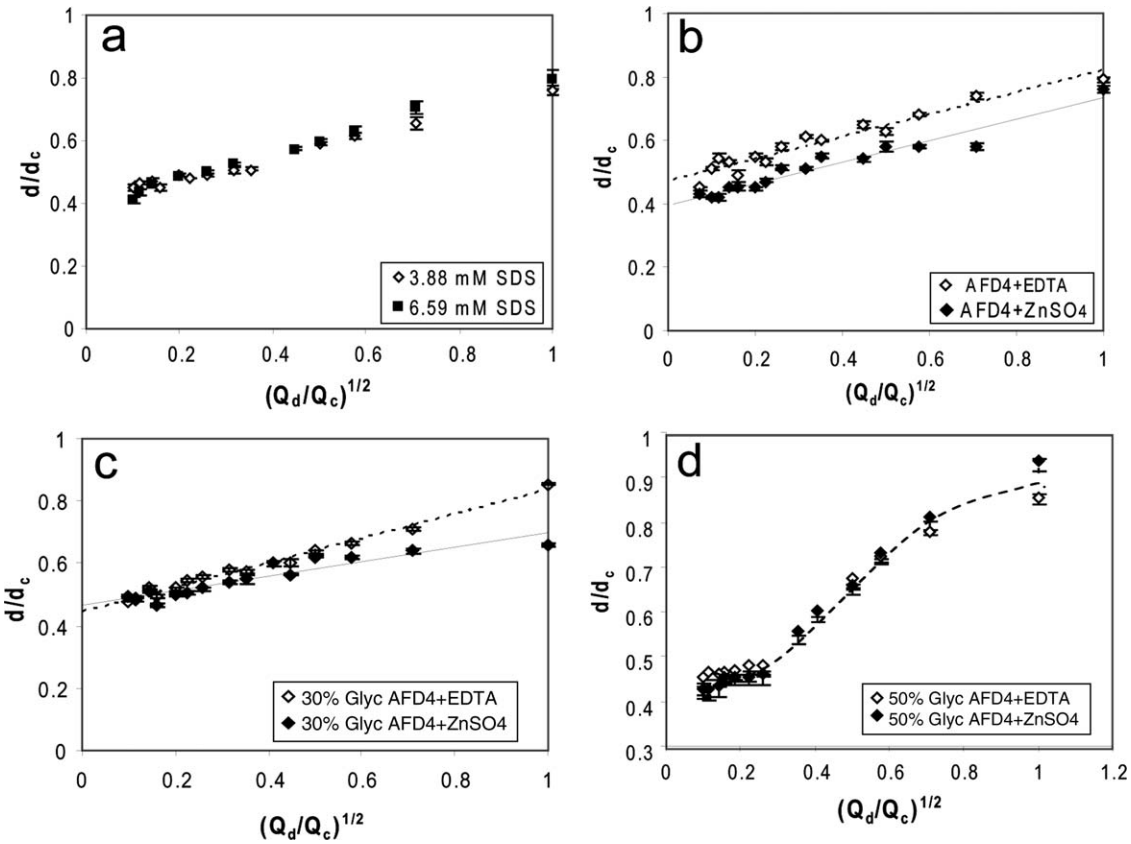


**Figure 8. Dimensionless droplet size versus $(Q_d/Q_c)^{1/2}$ with varied $Q_d$ (0.5, 0.1, and 0.02 mL/h) and $Q_c$ (0.5, 1.0,. 1.5, 2.0, and 4.0 mL/h).**

(a) SDS systems; (b) AFD4 systems; (c) 30% glycerol systems; (d) 50% glycerol systems. Viscosity ratios ($\alpha = \eta_c/\eta_d$ ) range from 5 to 30. Lines are to guide the eye only.

1.0, 1.5, 2.0, 4.0 mL/h) and dispersed phase (0.02, 0.1, 0.5 mL/h) flow rates (Table 2) were varied. Solutions containing the small molecular weight surfactant SDS (3.88 and 6.59 mM) were again used to vary the interfacial tension in a system lacking any significant interfacial elasticity. Peptide surfactants AFD4 and AM1 were compared to investigate the influence of elasticity on droplet size. It was found that the influence of interfacial tension on the final droplet size is negligible as seen in Figure 8a. Droplet size is well approximated by a power law relationship, as follows:

$$\frac{d}{d_c} \propto \left(\frac{Q_d}{Q_c}\right)^{1/2} \quad (1)$$

where $d$ is the droplet size, $d_c$ is the width of the main channel (400 $\mu$m) and $Q_d$ and $Q_c$ are the volumetric flow rates of the dispersed and continuous phases, respectively. Despite the similarities, distinct differences were observed for each of the six peptide surfactant systems. Systems AM1+EDTA and AFD4+EDTA, which have the lowest interfacial elasticity, produced the largest droplets. System AFD4+$ZnSO_4$ has the highest interfacial elasticity and led to the smallest droplet size; AM1+$ZnCl_2$, AM1+$ZnSO_4$ and AFD4+$ZnCl_2$ have intermediate interfacial elasticities and gave intermediate droplet sizes. The results for AFD4+EDTA and AFD4+$ZnSO_4$ are shown in Figure 8b as a typical example. For the six peptide systems, droplet size decreased with increasing interfacial elasticity, which is in agreement with the trend of decreasing droplet size with increasing interfacial elasticity for bulk emulsification in the presence of proteins that form a cohesive interfacial layer.[38]

The viscosity of the dispersed phase was also investigated by varying the concentration of glycerol in water, and the results are shown in Figures 8c, d. In the low-viscosity water systems, the difference in droplet size between AFD4+EDTA and AFD4+$ZnSO_4$ is significant over all the tested flow rate ratios. In contrast, for the 30% glycerol system, there is no significant difference in the droplet size at low $(Q_d/Q_c)^{1/2}$ ($\leq$0.2). Even though 30% Glyc AFD4+$ZnSO_4$ has very high elasticity (Table 2), the increased viscosity of the dispersed phase begins to dominate the interfacial elasticity difference. When the viscosity of the dispersed phase is further increased (50% glycerol), the viscosity effect begins to dominate the whole process across all accessible $Q_d/Q_c$ ratios. Droplet size for both AFD4+EDTA and AFD4+$ZnSO_4$ in 50% glycerol collapse onto one master curve independent of elasticity. The high interfacial elasticity of the 50% glycerol solutions is mainly due to the slowed adsorption of peptide surfactants in these very viscous phases, which creates large interfacial tension gradients

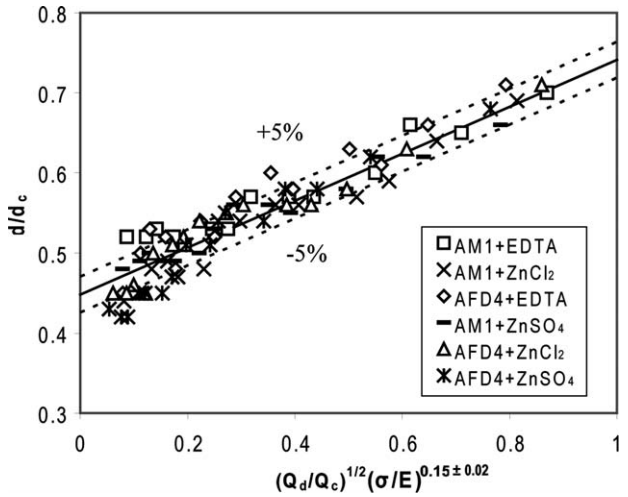


**Figure 9. Effect of interfacial elasticity on droplet size in microfluidic devices with varied $Q_d$ (0.5, 0.1 and 0.02 mL/h) and $Q_c$ (0.5, 1.0, 1.5, 2.0, and 4.0 mL/h).**

The plot shows dimensionless droplet size versus a new droplet size correlation incorporating a correcting term $\zeta$, which is the ratio of interfacial tension $\sigma$ to interfacial elasticity $E$ (values taken from Table 2).

which manifest as elasticity values by virtue of the PAT1 measurement technique, as discussed earlier.

Although considerable research has been undertaken to examine droplet formation processes in microfluidics, no correlations have previously emerged which allow a prediction of droplet size for surfactant systems which impart elasticity to droplet interfaces formed in microfluidic devices. Figure 9 shows a new correlation of droplet size as a function of the usual flow-rate ratio modified with a new group that is the ratio of interfacial tension and interfacial elasticity: $\zeta = \sigma/E$. Here $E$ is the interfacial dilatational elasticity measured with a PAT1 (Sinterface, Berlin, Germany) as reported in Table 2. Inclusion of the dimensionless parameter $\zeta$ collapsed nearly all the data for these six systems onto one curve with an error of approximately $\pm 5\%$ (Figure 9) for a range of $E$ between 2.83 and 39.0 mN/m.

## Conclusions

The results presented here reveal fundamental effects of interfacial elasticity on droplet formation in microfluidic devices. The presence of interfacial elasticity dramatically alters the dynamics of droplet breakup and affects secondary droplet formation in flow-focusing devices. Specifically, high interfacial elasticity delays neck thinning and creates a sharp pointed interface at breakup, while also suppressing the generation of secondary satellite droplets. Furthermore, high interfacial elasticity decreases final droplet size. We were able to quantitatively describe this effect by correlating droplet size as a function of a new dimensionless group, that being the square root of the flow-rate ratio multiplied by a dimensionless parameter $\zeta$, which accounts for the relative balance of interfacial tension and interfacial elasticity. The correlation was able to describe droplet size within 5%, despite order-of-magnitude changes in equilibrium interfacial elasticity.

## Acknowledgments

Financial support from the Australian Research Council (Grant DP0771910) is gratefully acknowledged. C.-X. Z. thanks Dr. Annette Dexter for her valuable discussions on the formulation and use of peptide surfactants. We thank the Australian National Fabrication Facility (ANFF) Queensland node for providing microfabrication facilities.

## Literature Cited

1. Charcosset C, Limayem I, Fessi H. The membrane emulsification process—a review. *J Chem Technol Biotechnol*. 2004;79:209–218.
2. Anna SL, Bontoux N, Stone HA. Formation of dispersions using "flow focusing" in microchannels. *Appl Phys Lett*. 2003;82:364–366.
3. Thorsen T, Roberts RW, Arnold FH, Quake SR. Dynamic pattern formation in a vesicle-generating microfluidic device. *Phys Rev Lett*. 2001;86:4163–4166.
4. Nisisako T, Torii T, Higuchi T. Droplet formation in a microchannel network. *Lab Chip*. 2002;2:24–26.
5. Van der Graaf S, Steegmans MLJ, van der Sman RGM, Schroen CGPH, Boom RM. Droplet formation in a T-shaped microchannel junction: a model system for membrane emulsification. *Colloids Surf A*. 2005;266:106–116.
6. Xu JH, Li SW, Tan J, Wang YJ, Luo GS. Preparation of highly monodisperse droplet in a T-junction microfluidic device. *AlChE J*. 2006;52:3005–3010.
7. Garstecki P, Fuerstman MJ, Stone HA, Whitesides GM. Formation of droplets and bubbles in a microfluidic T-junction—scaling and mechanism of break-up. *Lab Chip*. 2006;6:437–446.
8. Yobas L, Martens S, Ong WL, Ranganathan N. High-performance flow-focusing geometry for spontaneous generation of monodispersed droplets. *Lab Chip*. 2006;6:1073–1079.
9. Hamlington BD, Steinhaus B, Feng JJ, Link D, Shelley MJ, Shen AQ. Liquid crystal droplet production in a microfluidic device. *Liq Cryst*. 2007;34:861–870.
10. Xu QY, Nakajima M. The generation of highly monodisperse droplets through the breakup of hydrodynamically focused microthread in a microfluidic device. *Appl Phys Lett*. 2004;85:3726–3728.
11. Cramer C, Fischer P, Windhab EJ. Drop formation in a co-flowing ambient fluid. *Chem Eng Sci*. 2004;59:3045–3058.
12. Hua JS, Zhang BL, Lou J. Numerical simulation of microdroplet formation in coflowing immiscible liquids. *AIChE J*. 2007;53:2534–2548.
13. Hong YP, Wang FJ. Flow rate effect on droplet control in a co-flowing microfluidic device. *Microfluid Nanofluid*. 2007;3:341–346.
14. Kobayashi I, Nakajima M. Effect of emulsifiers on the preparation of food-grade oil-in-water emulsions using a straight-through extrusion filter. *Eur J Lipid Sci Technol*. 2002;104:720–727.
15. Kobayashi I, Nakajima M, Chun K, Kikuchi Y, Fukita H. Silicon array of elongated through-holes for monodisperse emulsion droplets. *AIChE J*. 2002;48:1639–1644.
16. Tan YC, Cristini V, Lee AP. Monodispersed microfluidic droplet generation by shear focusing microfluidic device. *Sens Actuators B*. 2006;114:350–356.
17. Garstecki P, Stone HA, Whitesides GM. Mechanism for flow-rate controlled breakup in confined geometries: a route to monodisperse emulsions. *Phys Rev Lett*. 2005;94:164501.
18. Kobayashi I, Mukataka S, Nakajima M. Effects of type and physical properties of oil phase on oil-in-water emulsion droplet formation in straight-through microchannel emulsification, experimental and CFD studies. *Langmuir*. 2005;21:5722–5730.
19. Dickinson E. Adsorbed protein layers at fluid interfaces: interactions, structure and surface rheology. *Colloids Surf B*. 1999;15:161–176.
20. Bateman JB, Chambers LA. "Surface elasticity" of protein films. I. Egg albumin. *J Chem Phys*. 1939;7:244–250.
21. Bateman JB, Chambers LA. "Surface elasticity" of protein films. II Properties of partially and of completely spread films. *J Phys Chem*. 1941;45:209–222.
22. Jones DB, Middelberg APJ. Direct determination of the mechanical properties of an interfacially adsorbed protein film. *Chem Eng Sci*. 2002;57:1711–1722.
23. Jones DB, Middelberg APJ. Interfacial protein networks and their impact on droplet breakup. *AIChE J*. 2003;49:1533–1541.

24. Middelberg APJ, Radke CJ, Blanch HW. Peptide interfacial adsorption is kinetically limited by the thermodynamic stability of self association. *PNAS*. 2000;97:5054–5059.
25. Middelberg APJ, He L, Dexter AF, Shen HH, Holt SA, Thomas RK. The interfacial structure and Young's modulus of peptide films having switchable mechanical properties. *J R Soc Interface*. 2008;5:47–54.
26. Dexter AF, Malcolm AS, Middelberg APJ. Reversible active switching of the mechanical properties of a peptide film at a fluid-fluid interface. *Nat Mater*. 2006;5:502–506.
27. Malcolm AS, Dexter AF, Katakdhond JA, Karakashev SI, Nguyen AV, Middelberg APJ. Tuneable control of interfacial rheology and emulsion coalescence. *Chemphyschem*. 2009;10:778–781.
28. Dexter AF, Middelberg APJ. Switchable peptide surfactants with designed metal binding capacity. *J Phys Chem C*. 2007;111:10484–10492.
29. Rodd LE, Cooper-White JJ, Boger DV, McKinley GH. Role of the elasticity number in the entry flow of dilute polymer solutions in micro-fabricated contraction geometries. *J Non-Newtonian Fluid Mech*. 2007;143:170–191.
30. He Q, Zhang Y, Lu G, Miller R, Mohwald H, Li JB. Dynamic adsorption and characterization of phospholipid and mixed phospholipid/protein layers at liquid/liquid interfaces. *Adv Colloid Interface Sci*. 2008;140:67–76.
31. Fainerman VB, Makievski AV, Miller R. The measurement of dynamic surface tensions of highly viscous-liquids by the maximum bubble pressure method. *Colloids Surf A*. 1993;75:229–235.
32. Malcolm AS, Dexter AF, Middelberg APJ. Mechanical properties of interfacial films formed by lysozyme self-assembly at the air-water interface. *Langmuir*. 2006;22:8897–8905.
33. Arratia PE, Gollub JP, Durian DJ. Polymeric filament thinning and breakup in microchannels. *Phys Rev E*. 2008;77:036309
34. Husny J, Cooper-White JJ. The effect of elasticity on drop creation in T-shaped microchannels. *J Non-Newtonian Fluid Mech*. 2006;137:121–136.
35. Tan YC, Lee AP. Microfluidic separation of satellite droplets as the basis of a monodispersed micron and submicron emulsification system. *Lab Chip*. 2005;5:1178–1183.
36. Zhang XG, Basaran OA. An experimental-study of dynamics of drop formation. *Phys Fluids*. 1995;7:1184–1203.
37. Tjahjadi M, Stone HA, Ottino JM. Satellite and subsatellite formation in capillary breakup. *J Fluid Mech*. 1992;243:297–317.
38. Dickinson E, Murray BS, Stainsby G. Time-dependent surface viscosity of adsorbed films of casein + gelatin at the oil-water interface. *J. Colloid Interface Sci*. 1985;106:259–262.

*Manuscript received Apr. 15, 2010, and revision received July 5, 2010.*